Performance evaluation of sinusoidal-flux reluctance machine for improving power density with reduced torque and input-current ripples

Kiwa Nagayasu, Masaki Iida, Kazuhiro Umetani, Masataka Ishihara, and Eiji Hiraki
Graduate school of natural science and technology,
Okayama University,
Okayama, Japan

Published in: 2022 24th European Conference on Power Electronics and Applications (EPE'22 ECCE Europe)

https://ieeexplore.ieee.org/document/9907173

Performance Evaluation of Sinusoidal-Flux Reluctance Machine for Improving Power Density with Reduced Torque and Input-Current Ripples

Kiwa Nagayasu, Masaki Iida, Kazuhiro Umetani, Mastaka Ishihara, Eiji Hiraki
OKAYAMA UNIVERSITY / GRADUATE SCHOOL OF NATURAL SCIENCE AND TECHNOLOGY
3-1-1 Tsushimanaka, Kita-ku
Okayama, Japan
Tel.: +81 / (86) – 251.8121.
Fax: +81 / (86) – 251.8115.
E-Mail: p4pg68f5@s.okayama-u.ac.jp
URL: https://www.cc.okayama-u.ac.jp/~eng_epc/

Acknowledgements

This study is supported by Nagamori Foundation Research Grant 2022.

Keywords

«Switched reluctance drive», «Electrical machine», «Ripple minimization», «Synchronous Reluctance Machine (SynRM)»

Abstract

Reluctance machines are attractive for vehicle propulsion for being free from the permanent magnets, although conventional reluctance machines, such as the synchronous reluctance machine (SynRM) and the switched reluctance machine (SRM), suffer from low power density or large input-current and torque ripples. To solve these problems, a recent study has proposed the sinusoidal-flux reluctance machine, which is operated with the sinusoidal phase flux waveform. This preceding study has confirmed the operating principle of this machine, although little information has been provided on the performance compared to the existing reluctance machines. The purpose of this study is to elucidate the benefits of the sinusoidal-flux reluctance machine compared to SynRM and SRM. This study experimentally tested the performance of the sinusoidal-flux reluctance machine, SynRM, and SRM, designed under the conditions of the same stator core and the same rotor outer diameter. The experiment revealed that the sinusoidal-flux reluctance machine can reduce the peak flux compared to the SynRM with smaller toque and input-current ripples than the SRM, suggesting that the sinusoidal-flux reluctance machine is promising for vehicle propulsion.

Introduction

Propelled by the recent concern about global warming, electrified vehicles, such as electric vehicles and hybrid vehicles, are attracting the researchers' attention for reducing the carbon dioxide emission. These vehicles are propelled by the electric machines installed in the body of the vehicle. As the vehicle propulsion needs to cover a wide range of driving conditions, these electric machines are required to be operated under a wide range of torque and rotation speed. Therefore, the majority of these electrified vehicles are currently adopting the permanent magnet synchronous machines (PSMS) [1]–[3] for propulsion systems, because they can offer large output torque at a comparatively small rotation speed, which is a difficult operation condition for many electric machines. However, these machines need permanent magnets, which suffer from expensive material costs and unstable material supply. Besides, the permanent magnets are mechanically fragile and thermally degradable, which requires the delicate mechanical design of the electric machines and a strong cooling system. These problems of the PMSMs may hinder the electrification of the low-cost vehicles, which are prevailing in number, particularly in developing countries, and therefore tend to have a great effect on carbon dioxide emission.

A possible approach to solve these problems is to adopt the reluctance machines for the propulsion of electrified vehicles. The reluctance machines do not need permanent magnets for their torque generating mechanism. Therefore, these machines can have simple but robust mechanical construction, high thermal tolerance, and strong cost-effectiveness, all of which are promising for installation in the vehicle. Therefore, many studies have investigated the application of the reluctance machines for vehicle propulsion [4]–[11]. The reluctance machines have a wide variety of mechanical structures and control schemes. However, the majority of these studies have focused on the two typical reluctance machines: The switched reluctance machine (SRM) [6], [7], [9] and the synchronous reluctance machine (SynRM) [8], [10], [11].

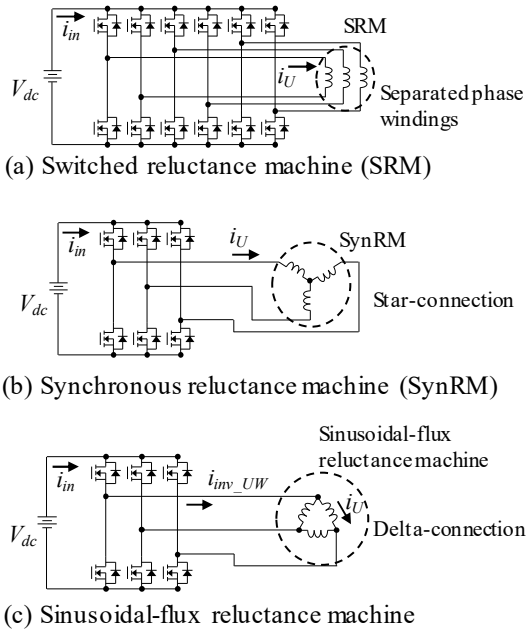

Fig. 1: Phase winding connection and inverter circuit of 3 reluctance machines

From the viewpoint of electric machine drive, the major difference between these two reluctance machines lies in the connection of the phase winding, the phase inductance (or reluctance) profile, and the phase current waveform to drive these machines. The SRM is designed to separate each phase winding from the others, as illustrated in Fig. 1(a). As shown later, the phase inductance was designed to have a triangular profile; the inverter should supply the phase current in the square waveform. The prominent merit of the SRM is the ability of comparatively larger torque output with smaller copper loss than SynRM, particularly at a low rotation speed. Contrarily, the SRM has severe drawbacks of the large input-current and torque ripples. The input-current ripple can deteriorate the battery lifespan due to the increase in the high-order harmonics in the battery current; the torque ripple can decrease the driving comfort due to the increase in the noise vibration. Therefore, the large input-current ripple and the large output torque ripple of the SynRM are severe drawbacks for vehicle propulsion. Another drawback of the SRM is that the normal three-phase inverters cannot be utilized to drive the SRM as the sum of the phase current is not zero [12]. Some recent studies [13][14] have certainly developed the control technique to greatly reduce both of the input-current and output torque ripples. However, even with these new technologies, the SRM does not accept the normal three-phase inverter, which entails a cost-up for the motor driving system.

On the other hand, the SynRM is designed to have the delta connection of the phase winding, as shown in Fig. 1(b), and the sinusoidal phase inductance profile. The inverter that drives this machine should supply the phase current in the sinusoidal waveform [15]. Theoretically, the SynRM can be operated without the input-current ripple and the output torque ripple. However, the SynRM tends to have low power density because the SynRM is susceptible to magnetic saturation due to the third harmonics contained in the phase flux density, as discussed in the subsequent section. Therefore, the size of the SynRM tends to be large for vehicle propulsion, hindering the installation in the limited space of vehicle.

As reviewed above, both of these two reluctance machines still have drawbacks for vehicular applications. To solve this difficulty, a novel reluctance machine concept has been proposed by recent studies [16][17]. Unlike the SynRM and the SRM, this machine has the phase windings connected in the delta connection, as shown in Fig. 1(c), the sinusoidal reluctance profile, and is driven with the sinusoidal phase flux waveform. Hereafter, this paper refers to this machine as the sinusoidal-flux reluctance machine. This machine is expected to operate without generating the input-current ripple and the output torque. Furthermore, this machine can be driven with the normal three-phase inverter. In addition to these attractive features, this machine can be operated with smaller peak phase flux and therefore can have greater power density than the SynRM.

The basic operating principles of the sinusoidal-flux reluctance machine have been experimentally and analytically confirmed in these preceding studies. However, the performance comparison with the SRM

and SynRM was not performed in these studies because the prototype of the sinusoidal-flux reluctance machine was not optimally designed for fair comparison with the SynRM and SRM. The purpose of this paper is to report the performance comparison results of the sinusoidal-flux reluctance machine with the SynRM and the SRM by fairly designing this reluctance machine under the same restrictions are SynRM and SRM. For observing the performance difference only by the basic operation principles, these three machines were designed only by changing the rotor outer periphery, winding connection, and number of the winding turns.

The remainder of this paper is divided into three sections. Section II briefly reviews the sinusoidal-flux reluctance machine in comparison with the SRM and the SynRM. Sections III and IV perform the simulation and the experiment, respectively, to confirm the performance of this reluctance machine in comparison with the SRM and the SynRM. Finally, section V gives the conclusions.

Review of Sinusoidal-Flux Machine in Comparison with SRM and SynRM

This section briefly reviews the operating principles of the sinusoidal-flux machine. For this purpose, the operating principles of SRM and SynRM are reviewed in advance. Hereafter, these reluctance machines are supposed to have the 3 phases, namely phases U, V, and W, as is common for these machines. The magnetic saturation is neglected in this section for simplifying the discussion.

In the reluctance machines, the phase inductance profile plays an essential role for electric energy conversion to the torque output. The phase inductance profile has the wavenumber of 2 when plotted as a function of the electric angle. The instantaneous torque τ and the input current i_{in} can be formulated as a function of the phase current i as,

$$\tau = \sum_{k=U,V,W} \frac{P}{2}\frac{dL_k}{d\theta} i_k^2, \quad i_{in} = \frac{1}{V_{dc}} \sum_{k=U,V,W} v_k i_k = \frac{1}{V_{dc}} \sum_{k=U,V,W} \frac{dL_k i_k}{dt} i_k = \frac{\Omega}{V_{dc}} \sum_{k=U,V,W} \left(2\tau + \frac{PL_k}{2}\frac{di_k^2}{d\theta} \right). \tag{1}$$

where P is the number of the rotor pole pairs; L is the phase inductance; θ is the electric angle; i is the phase current; V_{dc} is the voltage of the DC power supply to the inverter; v is the phase voltage; Ω is the angular velocity of the rotor, and subscription U, V, W are the indicator of the phase. On the other hand, the phase magnetic flux ϕ generated in a phase winding can be formulated as follows, if the number of turns of the phase winding denotes N:

$$\phi_k = L_k i_k / N. \tag{2}$$

The SRM has the triangular phase inductance profile. The phase windings are supplied with the square-shaped current with the same wavenumber as the inductance profile, as depicted in Fig. 2. The phase current flows for 60 degrees alternatingly in each phase during the increase of the phase inductance at a constant rate. Therefore, the constant torque and the constant input current are expected according to (1). However, the existence of the phase inductance prohibits the sharp drop of the phase current at the magnetizing and

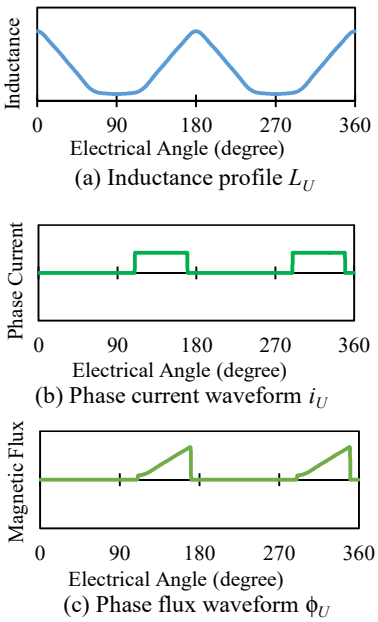

Fig. 2: Waveforms of SRM

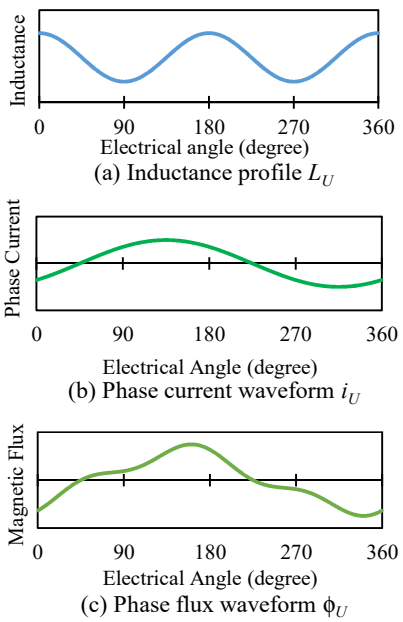

Fig. 3: Waveforms of SynRM

demagnetizing transients. Therefore, the actual phase current deviates from the ideal waveform, particularly at high rotating speed, causing large input-current and torque ripples.

On the other hand, the SynRM has the sinusoidal phase inductance profile as depicted in Fig. 3. The phase windings are supplied with the sinusoidal current waveform with the half wavenumber as the inductance profile. According to (1), this also results in the constant torque and the constant input current. Unlike the SRM, the phase current is not required to vary suddenly. Therefore, the SynRM can exhibit small input-current and torque ripples in a wide range of practical operations. However, according to (2), the magnetic flux waveform is not purely sinusoidal but contains the third harmonics. This harmonic increases the peak magnetic flux, although this harmonic does not contribute to the torque output. Therefore, the SynRM is susceptible to magnetic saturation, which restricts the maximum torque output and reduces the power density.

Unlike the SRM and the SynRM, the sinusoidal-flux reluctance machine has the sinusoidal phase reluctance profile, as depicted in Fig. 4, with the wavenumber of 2. Because the phase windings are connected in the delta-connection, each phase winding is applied with the sinusoidal voltage output from the inverter. Therefore, the phase magnetic flux has the sinusoidal waveform with the half wavenumber as the reluctance profile.

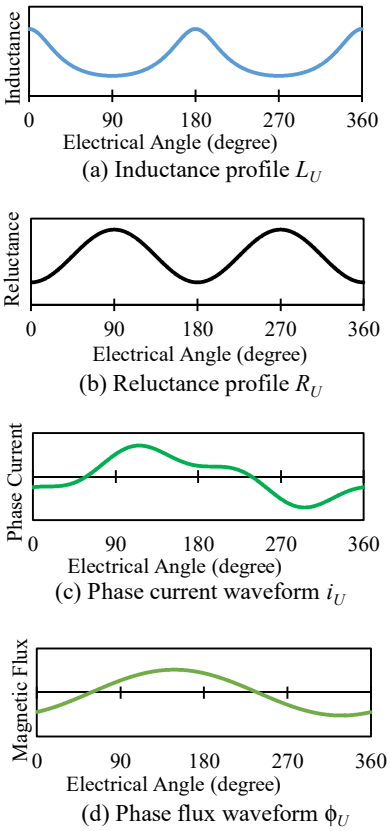

Fig. 4: Waveforms of sinusoidal-flux reluctance motor

Note that the phase reluctance R is formulated as $R=N^2/L$. Therefore, (1) can be rewritten as

$$\tau = -\sum_{k=U,V,W} \frac{P}{2}\frac{dR_k}{d\theta}\phi_k^2, \quad i_{in} = \frac{\Omega}{V_{dc}}\sum_{k=U,V,W} \frac{PR_k}{2}\frac{d\phi_k^2}{d\theta}. \tag{3}$$

Therefore, this machine also achieves the constant input current and the constant output torque, suggesting that this machine is beneficial in smaller input-current and torque ripples than SRM, similar to the SynRM. Furthermore, the phase magnetic flux waveform is purely sinusoidal without harmonics. Therefore, this machine is expected to have a smaller peak magnetic flux than the SynRM, which will result in an improvement in the maximum output torque and therefore the power density.

Despite the aforementioned attractive features, the phase current waveform of the sinusoidal-flux reluctance machine contains the third harmonics, which circulates in the delta-connected windings. Therefore, the inverter output current is sinusoidal without harmonics, similar to the SynRM, thus enabling the normal three-phase inverter to operate this machine. However, this circulating current can increase the copper loss compared to the SynRM, although the absence of the third harmonics in the phase magnetic flux will reduce the iron loss.

It is worth noticing that the phase flux waveform can have the phase shift from that depicted in Fig. 4, similar to the SynRM, which also accepts the phase shift of the phase current waveform from Fig. 3. The phase shift of the phase flux waveform does not increase the input-current nor torque ripples. Therefore, in practical design, the optimal phase shift can be designed under various design considerations. For example, the optimal phase shift can be determined so that the copper loss is minimized under the same torque output, which was adopted in the design of the sinusoidal-flux reluctance motor and the SynRM in the next section. Consequently, the sinusoidal-flux reluctance machine can avoid the drawbacks of the SynRM and the SRM.

Simulation-Based Design of Sinusoidal-Flux Reluctance Machine

Table I: Specifications of Commercial SRM

Model number	RB165SR-96CSRM (Motion System Tech Inc.)
Rated value	1.2 kW, 96V, 6000 r/min
Pole number	Stator: 12 poles, Rotor: 8 poles
Number of turns	14 turns/pole
Min. gap b/w stator and rotor	0.3 mm
Stack length	40 mm

For performance comparison of the three reluctance machines, i.e. the proposed machine, the SynRM, and the SRM, these machines were designed by utilizing the electromagnetic simulator JMAG19.1 (JSOL Corp.). The three reluctance machine models were constructed based on the commercially available SRM, which is used as the SRM. The specifications of the SRM are listed in Table I. All machine models have the same stator with concentrated windings. However, the number of turns was different depending on the connection of the phase winding: The number of turns was set at 14 for the SynRM and the SRM, whereas the number of turns was set at 24 for the sinusoidal-flux reluctance machine because the voltage applied to the phase winding is $\sqrt{3}$ times greater than that of the SynRM due to the delta-connection. Beside of the number of turns, the only difference lies in the rotor shape. Commonly SynRMs have a rotor shape with multiple flux barriers. However, for simplifying the difference among the three machines, we designed the rotors of the proposed reluctance machine and the SynRM by only modifying the rotor's outer periphery shape of the commercial SRM without implementing the flux barriers.

Design of Rotor Geometry

The rotor geometry of the sinusoidal-flux reluctance machine and the SynRM was determined by approximating the rotor geometry by a 288-gon and optimizing the gap length between each vertex and the inner diameter of the stator. This section hereafter describes the rotor geometry determination process of the sinusoidal-flux reluctance machine, although a similar procedure was also taken to determine the rotor geometry for the SynRM.

According to the preceding study [16], the design of the sinusoidal-flux reluctance machine should consider the following two points to have good efficiency: 1. The maximum phase inductance, i.e. the inductance at the aligned position, should have as great value as possible; 2. The ratio of the maximum phase reluctance to the least phase reluctance should be around 3. Therefore, this study designed the rotor shape according to these instructions.

As the sinusoidal-flux reluctance machine should be designed to have the sinusoidal phase reluctance profile, a straightforward method for designing the rotor geometry is to determine the gap length $l_p(\theta)$ from the rotor outer periphery to the stator inner diameter by the sinusoidal wave with the wavenumber of 2. Hence, $l_p(\theta)$ is determined by the following equation, where l_{p0} and l_{p1} are the positive values determined by the design.

$$l_p(\theta) = l_{p0} - l_{p1}\cos 2\theta. \tag{4}$$

According to the instruction the gap length at the aligned position, i.e. $l_{p0}-l_{p1}$ should be set at the minimum possible gap length accepted by the mechanical restrictions; l_{p1} should be set to have the appropriate value of the ratio between the maximum and minimum reluctance. However, this straightforward design resulted in the reduction of the maximum inductance because the gap $l_p(\theta)$ starts to increase at any small deviation from the aligned position, i.e. θ=0°, 180°. Therefore, for maximizing the inductance at the aligned position, the increase of the gap length should be suppressed near the aligned position. For this purpose, this paper determined $l_p(\theta)$ according to the following equation where l_{p2} is an additional value to be determined by design:

$$l_p(\theta) = l_{p0} - l_{p1}\cos 2\theta + l_{p2}\cos 4\theta. \tag{5}$$

As can be seen in Fig. 5, this function can suppress the gap length increase near the aligned position to increase the maximum inductance. Nonetheless, adding the third right-hand term causes deviation of the phase reluctance profile from the sinusoidal waveform, increasing the input-current and torque ripples. Therefore, l_{p0}, l_{p1}, and l_{p2} should be determined to increase the maximum phase inductance at the aligned position while considering the acceptable ripples. This paper adopted the input-current ripple ratio of 200% and the torque ripple ratio of 80% as the acceptable ripple rations, where the ripple ratio is defined as the difference between the maximum and minimum values normalized by the average value. These acceptable ripple ratios were set to be below the commercial SRM. This design may be far from an optimal design. Better design for the sinusoidal-flux reluctance machine should be sought in future studies.

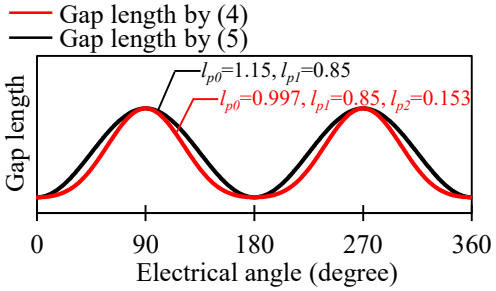

Fig.5 :Comparison of gap lengths in (4) and (5) in the sinusoidal-flux reluctance machine

The gap length at the aligned position, i.e. $l_{p0}-l_{p1}+l_{p2}$, was set at 0.3mm, which is the minimum gap length of the commercial SRM. Under this restriction, the optimal values for three parameters l_{p0}, l_{p1}, and l_{p2} were searched according to the flowchart shown in Fig. 6. This flowchart indicates the trial-and-error approach for designing these parameters. Initial parameters were determined by setting l_{p2} at zero: $L_{p0} = 0.8$, $L_{p1} = -0.5$, and $L_{p2} = 0.0$. Firstly, the rotor shape was designed for l_{p0}, l_{p1}, and l_{p2} using 3D CAD design software (Fusion360). Based on this rotor shape, the inductance profile $L_U(\theta)$ was calculated using the electromagnetic field simulator (JMAG-Designer). Based on this result, the optimal phase shift angle of the phase flux was analytically calculated so that the output torque or 1Nm was output with the smallest copper loss. Then the input-current and torque ripples were calculated to check whether these ripples are within the acceptable ripple ratios. By repeating this process while gradually increasing l_{p2}, the optimal design of the rotor shape was determined as $L_{p0} = 0.997$, $L_{p1} = -0.85$, and $L_{p2} = 0.153$, which has the minimum copper loss within the acceptable ripple ratios.

Simulation Results

To confirm the design of the sinusoidal-flux reluctance machine, the electromagnetic field simulation was carried out using the simulator JMAG (JSOL Corp.). This simulation tested the design of the three reluctance machines, i.e. the sinusoidal-flux reluctance machine, the SynRM, and the SRM. Figure 7 shows the simulation models of these three machines; Table 2 lists the materials adopted for the simulation models, although the magnetic saturation was not considered in this simulation.

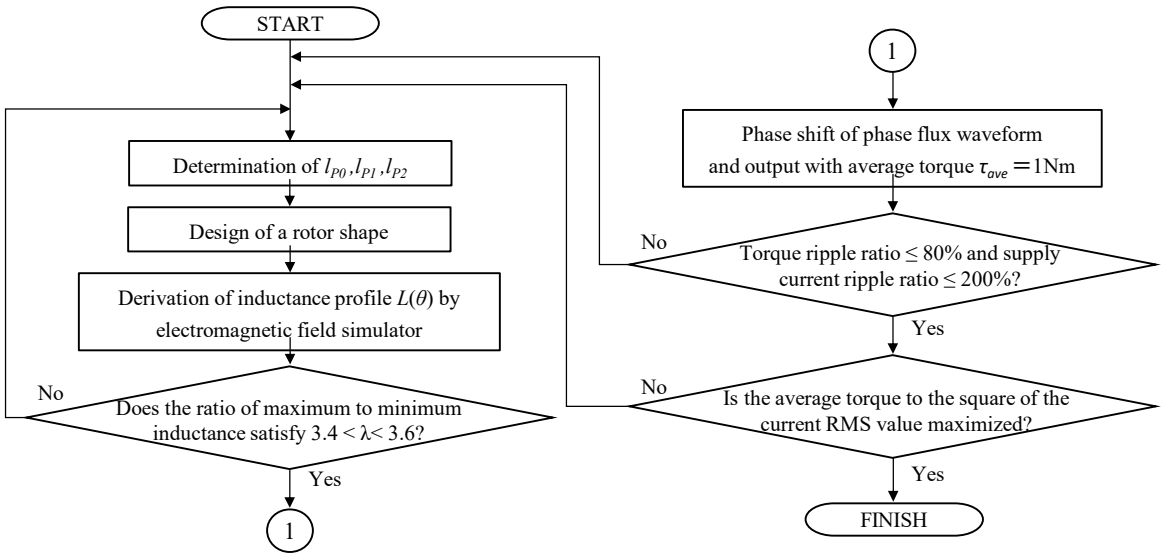

Fig.6 : Design algorithm for the rotor geometry of the sinusoidal-flux reluctance machine

Table II: Materials used in FEM model

Component	Material or relative magnetic permeability
Stator	Material name: 35H300 (Nippon Steel Corp.)
Rotor	Material name: 35H300 (Nippon Steel Corp.)
Winding	Relative magnetic permeability: 1
Shaft	Relative magnetic permeability: 1

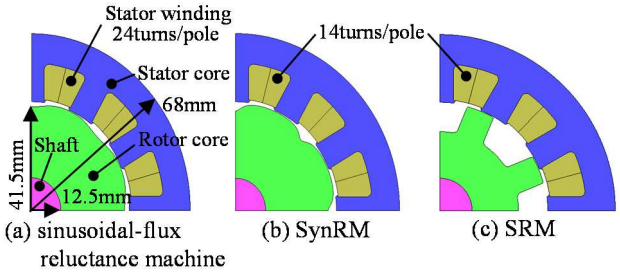

Fig. 7: Electromagnetic simulation models

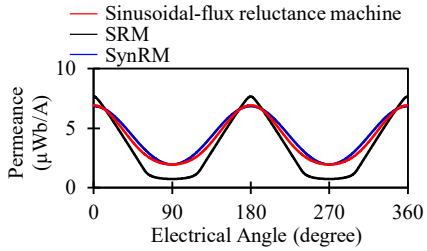

Fig. 8: Permeance profile for simulation

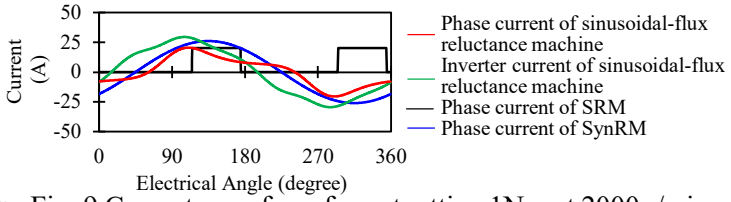

Fig. 9 Current waveform for outputting 1Nm at 2000 r/min

Figure 8 shows the permeance of the three reluctance machines. This figure plots the permeance profile instead of the inductance profile because the number of turns of the phase windings is different among the three machines due to the difference in the phase winding connection. The results revealed that the sinusoidal-flux reluctance machine exhibited maximum permeance similar to the SynRM but slightly smaller than the SRM. The ratio between the maximum and minimum inductance was 3.5 in the sinusoidal-flux reluctance machine, which was within the target of the design.

Based on the permeance profile calculated in Fig. 8, a motor behavior model was constructed to calculate the input-current and torque ripples by utilizing the inverter circuit simulator. For this purpose, the behavior models of the three reluctance machines were constructed according to [18] and operated using the driving systems shown in Fig. 1, which were modeled in the model space of the circuit simulator PSIM2021a (Myway Corp.). The inverters of the driving systems were supplied with the DC power of the voltage Vdc=96 V. This simulation did not contain any losses and consider the magnetic saturation.

The inverter output current was controlled by the hysteresis control with the hysteresis width of 0.5 A to follow the current command values. Figure 9 shows the command values for 1 Nm at 2000 r/min.

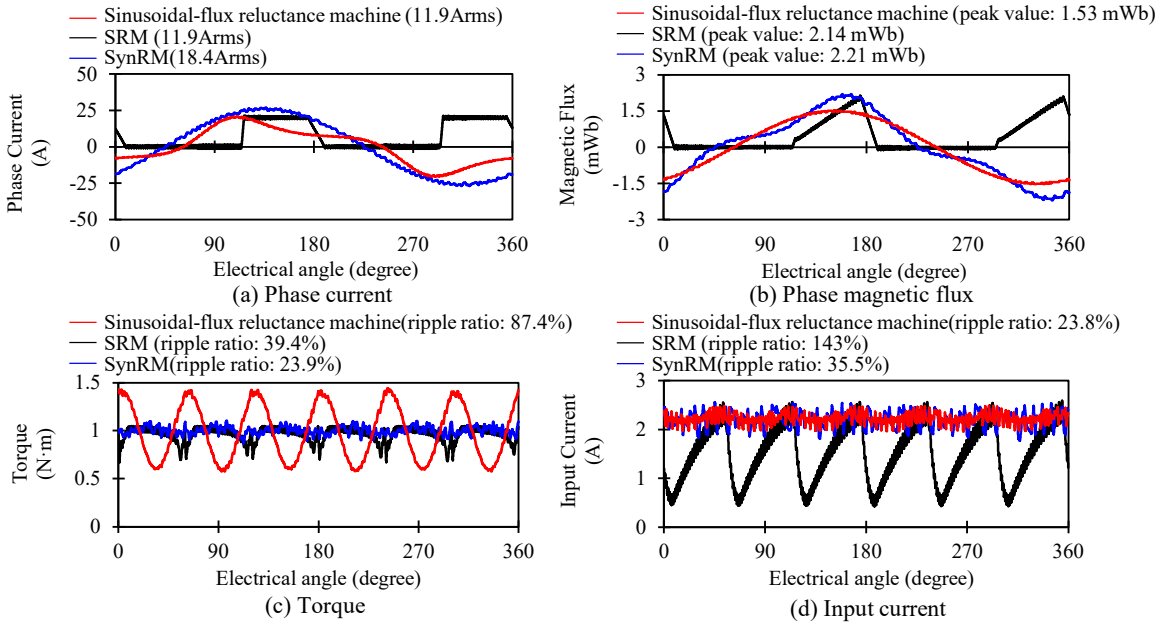

Fig. 10: Simulation results of operations at 1 Nm, 2000 r/min

Figure 10 shows the simulation results at the output torque of 1 Nm and the rotation speed of 2000 r/min. As can be seen in the figure, the sinusoidal-flux reluctance machine exhibited the smallest peak magnetic flux, which is a promising feature to mitigate the magnetic saturation and improve the power density. As for the phase current waveforms, the sinusoidal-flux reluctance machine exhibited the smallest rms values. However, this is because this machine has much greater number of turns, i.e. 24 turns, compared to the SynRM and the SRM, which has the 14 turns. If the resistance of the phase winding is simply approximated to be proportional to the square of the number of turns, the copper loss of the sinusoidal-flux reluctance machine is 1.22 times greater than the SynRM and 2.94 times greater than the SRM.

(a) Sinusoidal-flux reluctance machine (b) SynRM (c) SRM

Fig. 11: Photographs of rotors of experimental reluctance machines

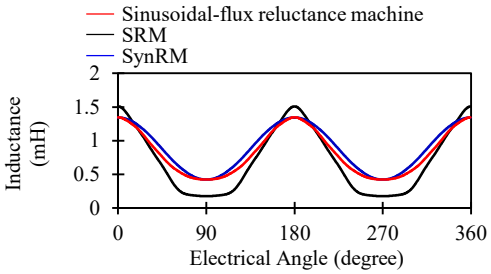

Fig. 12: Measurement result of the inductance profile

This figure also shows the simulation results of the input-current and torque ripples. The sinusoidal-flux reluctance machine exhibited a significant torque ripple. This may have been caused by the insufficient optimization of the rotor geometry, which should be improved in future study. However, the sinusoidal-flux reluctance machine exhibited a small input-current ripple similar to the SynRM, which is far smaller than the SRM. Therefore, the simulation results imply the potential power density improvement by the sinusoidal-flux reluctance machine in comparison to the SynRM with a increase in the copper loss, although the further design optimization method of the rotor geometry should be investigated to reduce the torque ripple to the similar value as the SynRM.

Experiment

The experiment was carried out to test the performance of the sinusoidal-flux reluctance machine in comparison with the SRM and the SynRM. The SRM and the SynRM incorporated the same stator with the phase windings of 14 turns, which is the stator of the commercial SRM specified in Table I. The sinusoidal-flux reluctance machine also adopts the same stator except that the number of the phase winding is changed to 24. The rotors of these machines were fabricated according to the design obtained in the previous section. Figure 11 shows the photographs of the rotors. These electric machines exhibited inductance profiles similar to the simulation result of the previous section, as shown in Fig. 12. The current command values for the inverters were determined based on Fig. 12.

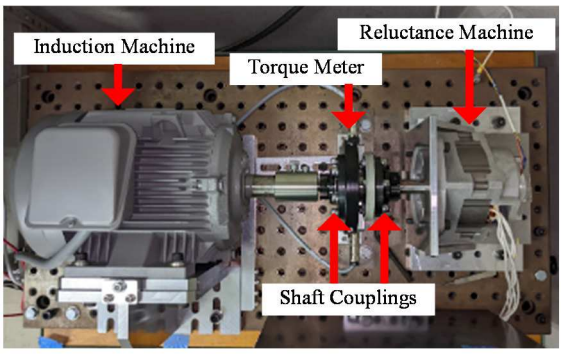

Fig. 13: Machine test bench

Table III : List of Motor Bench

Used equipment	Model No,(manufacturer)
Motor for measurement	RB165SR-96CSRM (Motion System Tech Inc.)
Torque meter	T40B (HBM Co.)
Induction Machine	TFO-K(Hitachi, Ltd.)

Table IV : List of used equipment

Used equipment	Model No.(Manufacturer)
Oscilloscope	HDO4034A (Teledyne LeCroy)
Current Probe Amplifier	TCPA300 (Tektronix, Inc)
Current Probe(i_{in})	TCP305A (Tektronix, Inc)
Current Probe(i_U)	TCP303 (Tektronix, Inc)
High Voltage Differential Probe(v_U)	P5200A (Tektronix, Inc)
DC power supply(V_{dc})	GP0110-50R (Takasago, Ltd)
Digital multimeter(Measurement of V_{dc})	34461A (Keysight Technologies)

In this experiment, the operating waveforms of the sinusoidal-flux machine, SynRM, and SRM were evaluated using the reluctance machine test bench shown in Fig. 13. The specifications of the test bench are listed in Table III. In this test bench, the reluctance machine was mechanically connected to the induction machine, which serves as the power load, via an instantaneous torque meter and coupling. The reluctance machine was supplied with ac power via an inverter according to the circuit diagram shown in Fig. 1. The inverter was supplied with the dc voltage of 96 V. The inverter was controlled to output the ac current according to the current command value using the same hysteresis control as described in the previous section. The hysteresis width was adjusted to operate these experimental electric machines approximately at the inverter switching frequency of 30kHz.

Firstly, the operating waveforms were measured under two driving conditions corresponding to the unsaturated magnetization and the saturated magnetization of the sinusoidal-flux reluctance machine. Specifically, the former condition outputs the torque of 1 Nm, whereas the latter condition outputs the torque of 4 Nm. Similar to the simulation, the experiment evaluated the following four waveforms: 1. Phase current, 2. Phase voltage, 3. Input current, and 4. Instantaneous torque. Table IV lists the instrument employed for the measurement. The phase current, phase voltage, and input current were measured at the rotation speed of 2000 r/min. However, the instantaneous torque was measured at the rotation speed of 100 r/min for the torque ripple to be within the frequency range of the instantaneous torque meter and not to induce the mechanical resonance of the motor test bench.

Figure 14 shows the operating waveforms of the three reluctance machines, measured at the output torque of 1 Nm. The peak phase flux of the sinusoidal-flux reluctance machine was found to be the smallest among the three electric machines. Specifically, the maximum phase flux of the sinusoidal-flux reluctance machine was 20% smaller than that of the SynRM, indicating that the sinusoidal-flux machine is less susceptible to magnetic saturation. The sinusoidal-flux reluctance machine exhibited the effective reduction of the input current ripple compared to the SRM, as is similar to the SynRM. Meanwhile, the sinusoidal-flux reluctance machine did not show an effective reduction of the torque ripple. As discussed in the simulation, this insufficient reduction effect of the torque ripple was caused by the insufficient design optimization of the sinusoidal-flux reluctance machine, which will be investigated in the future study.

Figure 15 shows the operating waveforms at the output torque of 4 Nm. In this condition, the sinusoidal-flux reluctance machine again exhibited the smallest peak phase flux among the three machines. Furthermore, this machine also exhibited the smallest input-current ripple and a similar torque ripple as the SynRM. Therefore, the sinusoidal-flux reluctance machine kept the input-current and torque ripples

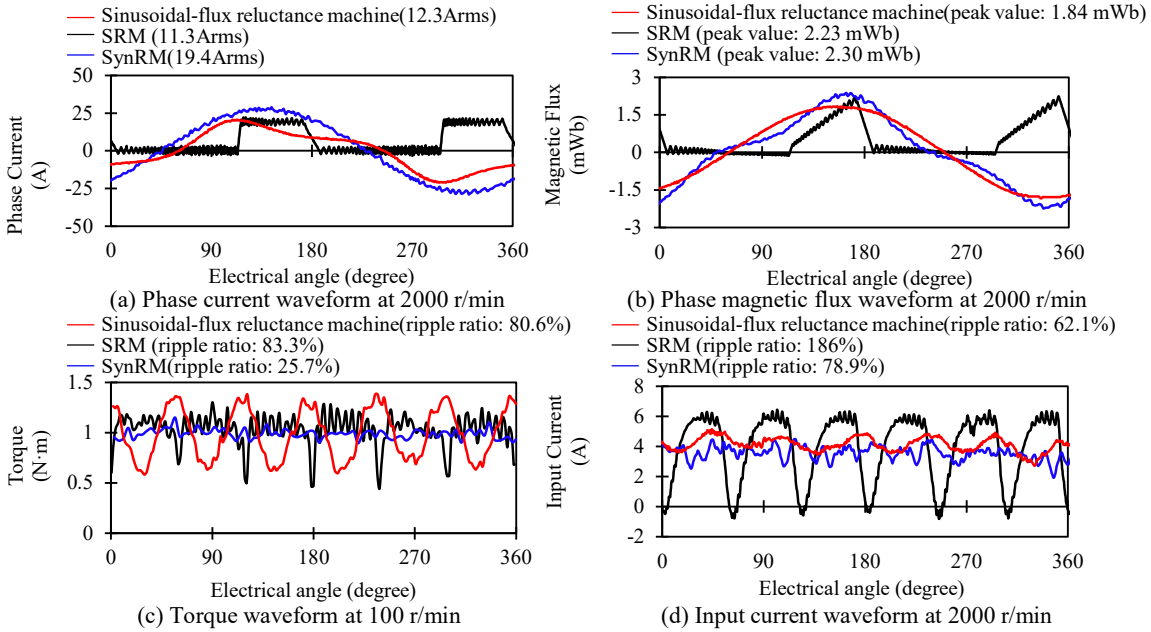

(a) Phase current waveform at 2000 r/min
(b) Phase magnetic flux waveform at 2000 r/min
(c) Torque waveform at 100 r/min
(d) Input current waveform at 2000 r/min
Fig.14: Experimental results of operations at 1 Nm

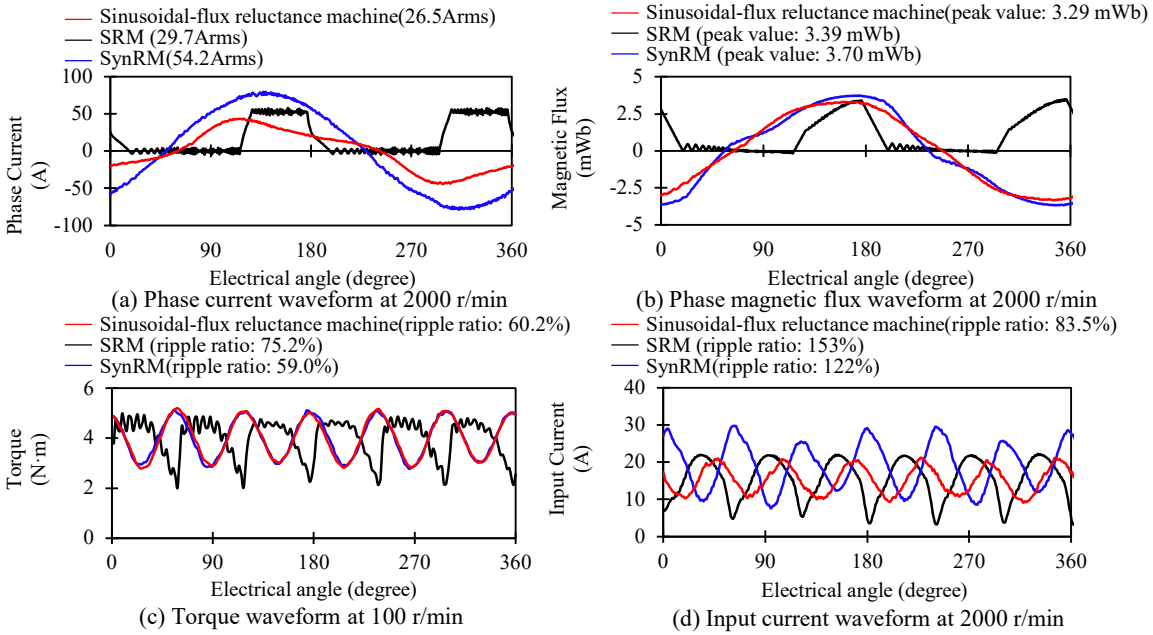

(a) Phase current waveform at 2000 r/min

(b) Phase magnetic flux waveform at 2000 r/min

(c) Torque waveform at 100 r/min

(d) Input current waveform at 2000 r/min

Fig. 15: Experimental results of operations at 4 Nm

small even under high torque output, whereas the SynRM increased rapidly the input-current and torque ripples as the output torque increases. The reason for this difference lies in maximum phase flux. Because the SynRM generates a large phase flux than the sinusoidal-flux reluctance machine, the SynRM tends to increase the ripples at lower output torque than the sinusoidal-flux reluctance machine. Therefore, these results support that the sinusoidal-flux reluctance machine can improve the power density compared to the SynRM.

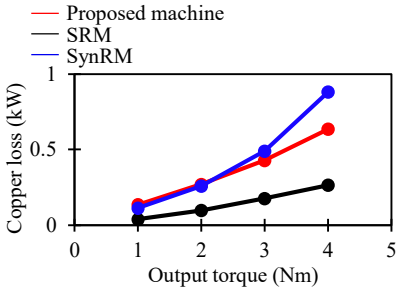

Fig. 16: Comparison of copper loss at various output torque

The simulation results reported in the previous section pointed out that the major drawback of the sinusoidal-flux reluctance machine is large copper loss. Therefore, the rms values of the phase current were evaluated at various output torque to estimate the copper loss of the phase windings and compare the result among the three reluctance machines. Figure 16 presents the results. Certainly, the sinusoidal-flux reluctance machine exhibited far greater copper loss than the SRM, similarly to the SynRM. However, if compared to the SynRM, the sinusoidal-flux reluctance machine exhibited less copper loss at high output torque operation. This is also caused by the reduction in the peak phase flux. Because the SynRM more profoundly saturates than the sinusoidal-flux reluctance machine, the SynRM tends to generate large copper loss at high output torque operations. Therefore, this result also supports that the sinusoidal-flux reluctance machine can improve the power density compared to the SynRM.

Conclusions

Reluctance machines are attractive for vehicular propulsion, although conventional reluctance machines as the SynRM and the SRM suffers from low power density or large input-current and torque ripples. To overcome these difficulties, the novel reluctance machine with sinusoidal phase flux has been recently proposed. This paper constructed this reluctance machine and tested the performance in comparison with the SynRM and the SRM using the simulation and the experiment. The sinusoidal-flux reluctance machine and the SynRM were designed from the commercially available SRM, which was used as the SRM, by only changing the rotor outer periphery geometry and the number of turns of the phase windings, in order to examine the features originated from the fundamental concept of these three reluctance machines. The simulation and experiment indicated that the sinusoidal-flux reluctance machine can generate a far smaller input-current ripple than the SRM. Furthermore, the sinusoidal-flux reluctance machine was found to reduce the peak phase flux compared to the SynRM. The experiment

also supported that the sinusoidal-flux reluctance machine generates similar torque ripple and smaller input-current ripple with smaller copper loss compared to the SynRM at high output torque operation, which suggests the power density improvement by the sinusoidal-flux reluctance machine. At the same time, however, the sinusoidal-flux reluctance machine exhibited a large torque ripple similar to the SRM, which is unexpected from the theory. This discrepancy from the theory is attributed to the insufficient rotor design of the sinusoidal-flux reluctance machine. Therefore, better rotor shape design should be investigated in a future study to reduce the torque ripple.

References

[1] Du J. Wang X., Lu H.: Optimization of magnet shape based on efficiency map of IPSMS for EVs, IEEE Trans. Appl. Supercond, vol. 26, no. 7, pp. 1-7, Oct. 2016, Art no. 0609807.

[2] Jung. H., Park G., Kim D., Jung S.: Optimal design and validation of IPMSM for maximum efficiency distribution compatible to energy consumption areas of HD-EV, IEEE Trans. Magn., vol. 53, no. 6, pp. 1-4, Jun. 2017, Art no. 8201904.

[3] Hwang Y., Lee J.: HEV motor comparison of IPMSM with Nd sintered magnet and heavy rare-earth free injection magnet in the same size, IEEE Trans. Appl. Supercond., vol. 28, no. 3, pp. 1-5, Apr. 2018, Art no. 5206405.

[4] Zhu Z. Q., Chan C. C.: Electrical machine topologies and technologies for electric, hybrid, and fuel cell vehicles, Proc. IEEE Vehicle Power Propulsion Conf., Harbin, China, pp. 1–6, Sept. 2008.

[5] Raminosoa T. Torrey D. A., El-Refaie A. M., Grace K., Pan D., Grubic S., Bodla K., Huh K.-K.: Sinusoidal reluctance machine with dc winding: an attractive non-permanent-magnet option, IEEE Trans. Ind. Appl., vol. 52, no. 3, pp. 2129-2137, May/Jun. 2016.

[6] Uddin W., Husain T., Sozer Y., Husain I.: Design methodology of a switched reluctance machine for off-road vehicle applications, IEEE Trans. Ind. Appl., vol. 52, no. 3, pp. 2138-2147, May/Jun. 2016.

[7] Martin R., Widmer J. D., Mecrow B. C., Kimiabeigi M., Mebarki A., Brown N. L.: Electromagnetic considerations for a six-phase switched reluctance motor driven by a three-phase inverter, vol. 52, no. 5, pp. 3787-3795, Sept./Oct. 2016.

[8] Bianchi N., Bolognani S., Carraro E., Castiello M.: Electric vehicle traction based on synchronous reluctance motors, IEEE Trans. Ind. Appl., vol. 52, no. 6, pp. 4762-4769, Nov./Dec. 2016.

[9] Zhu J., Cheng K. W. E., Xue X., Zou Y.: Design of a new enhanced torque in-wheel switched reluctance motor with divided teeth for electic vehicles, IEEE Trans. Magn., vol. 53, no. 11, pp. 1-4, Nov. 2017, Art no. 2501504.

[10] Kumar G. V., Chuang C.-H., Lu M.-Z., Liaw C.-M.: Development of an electric vehicle synchronous reluctance motor drive, IEEE Trans. Vehicular Tech., vol. 69, no. 5, pp. 5012-5025, May 2020.

[11] Credo A., Fabri G., Villani M., Popescu M.: Adopting the topology optimization in the design of high-speed synchronous reluctance motors for electric vehicles, IEEE Trans. Ind. Appl., vol. 56, no. 5, pp. 5429-5438, Sept./Oct. 2020.

[12] Suppharangsan W., Wang J.: Experimental validation of a new switching technique for DC-link capacitor minimization in switched reluctance machine drives, Proc. IEEE Int. Electric Machines Drives Conf., Chicago, USA, pp. 1031–1036, May 2013.

[13] Kusumi T., Hara T., Umetani K., Hiraki E.: Phase-current waveform for switched reluctance motors to eliminate input-current ripple and torque ripple in low-power propulsion below magnetic saturation, IET Power Electronics, vol. 13, no. 15, pp. 3351–3359, Nov. 2020.

[14] Kusumi T., Hara T., Umetani K., Hiraki E.: Simultaneous tuning of rotor shape and phase current of switched reluctance motors for eliminating input current and torque ripples with reduced copper loss, IEEE Trans. Ind. Appl., vol. 56, no. 6, pp. 6384–6398, Nov. 2020.

[15] Payza O., Demir Y., Aydin M.: Investigation of losses for a concentrated winding high-speed permanent magnet-assisted synchronous reluctance motor for washing machine application, IEEE Trans. Magn., vol. 54, no.11, 8207606, 2018.

[16] Iida M., Kusumi T., Umetani K., Hiraki E.: Feasibility of sinusoidal flux drive design of switched reluctance motor for reducing torque and input current ripples with three-leg inverter, Proc. IEEE Intl. Power Electron. Motion Ctrl. Conf. (PEMC2020), Apr.2020, Gliwice, Poland, pp. 439–446.

[17] Iida M., Umetani K., Kusumi T., Ishihara M., Hiraki E.: Sinusoidal-flux reluctance machine driven with three-phase inverter for improving power density with reduced torque and input current ripples, Proc. IEEE European Conf. Power Electron. Appl.(EPE2021), Ghent, Belgium, Sept. 2021, pp., 1–10.

[18] Hara T., Kusumi T., Umetani K., Hiraki E.: A simple behavior model for switched reluctance motors based on magnetic energy, Proc. Intl. Power Electron. Motion Control Conf. (IPEMC2016), Hefei, China, May. 2016.